

Track to Reconstruct and Reconstruct to Track

Jonathon Luiten^{*1}, Tobias Fischer^{*1} and Bastian Leibe¹

Abstract—Object tracking and reconstruction are often performed together, with tracking used as input for 3D reconstruction. However, the obtained 3D reconstructions also provide useful information that can be exploited to improve tracking. In this paper, we propose a novel method that closes this loop, tracking to reconstruct, and then reconstructing to track. Our approach, MOTSFusion (Multi-Object Tracking, Segmentation and dynamic object Fusion), exploits the 3D motion extracted from dynamic object reconstructions to track objects through long periods of complete occlusion and to recover missing detections. For this, we build up short tracklets using the 2D motion consistency of segmentation masks under optical flow warping. These tracklets are then fused into dynamic 3D object reconstructions which define the precise 3D motion. This 3D motion is used to merge tracklets into long-term tracks, even when objects are completely occluded for up to 20 frames, and to locate objects when detections are missing. On the KITTI dataset, our reconstruction-based tracking reduces the number of ID switches of the initial tracklets by more than 50%. This large improvement in long-term tracking ability results in MOTSFusion outperforming previous approaches in both bounding box and segmentation mask tracking accuracy.

I. INTRODUCTION

Multi-Object Tracking (MOT) is the task of localizing objects in a video and assigning consistent IDs to these objects so that each instance of the same object is always given the same ID. This task is crucial for applications such as autonomous vehicles and mobile robots, which need to understand the presence, location and motion of dynamic objects. MOT methods need to track objects both in frames where the objects are contiguously present, as well as through long periods where the objects are not visible due to occlusion. Many current MOT approaches focus on the first part, successfully tracking objects when they are consistently visible, but fail to track objects long-term through disappearance and occlusion, assigning incorrect IDs to objects when they reappear. However, accurate long-term tracking is crucial for understanding complex scenes to the levels required for fully autonomous systems.

To tackle long-term tracking, we propose to use dynamic 3D reconstructions to estimate the 3D motion of objects. Using this motion information, it is possible to track objects through occlusion and to recover missing detections, greatly improving long-term tracking results. Our algorithm closes the tracking-reconstruction loop, building reconstructions from tracks, and then improving tracking using these reconstructions.

^{*}Equal Contribution

¹Computer Vision Group, RWTH Aachen University, Germany. {luiten, leibe}@vision.rwth-aachen.de tobias.fischer@rwth-aachen.de

Code available: <https://github.com/tobiasfshr/MOTSFusion>



Fig. 1. **Qualitative results of our dynamic 3D reconstruction based tracking.** Top: Global scene reconstruction with the 3D bounding boxes for each object track in world coordinates. Bottom: Result of our dynamic object reconstruction, for three of the object tracks in the top image.

We present MOTSFusion (Multi-Object Tracking, Segmentation and dynamic object Fusion), a novel MOT method which produces segmentation masks as well as dynamic 3D object reconstructions and localizations. An example of this dynamic 3D reconstruction based tracking can be seen in Figure 1. MOTSFusion consists of a two-stage tracking pipeline. First, we associate bounding box detections into short spatio-temporally consistent tracklets in the image domain by calculating a segmentation mask for each detection and measuring the consistency of these masks under a warp defined by the optical flow. In the second stage of our algorithm, we project these tracklets into a global 3D domain using the camera ego-motion and a per pixel depth estimate. For each tracklet, a set of homogeneous transformations are calculated which align the object representations at each timestep into a dynamic reconstruction, defining the precise 3D motion of the object. Visual results of this stage are shown in Figure 2. For each tracklet, we extrapolate the 3D motion prediction that was obtained from this precise alignment. We merge tracklets into long-term object tracks by comparing the estimated 3D motion consistency of each tracklet. Our tracking results bridge occlusions and missing detections of up to 20 frames. Finally, we fill in missing detections and segmentation masks using the estimated positions from our 3D tracklet motion extrapolation. In this way our tracker is able to exploit both 2D image space motion consistency (using optical flow and segmentation masks), and 3D world-space motion consistency (using dynamic 3D reconstructions from depth and ego-motion estimates) for accurate long-term tracking.

In order to fuse dynamic objects in 3D, MOTSFusion relies on the assumption that the objects to be tracked only move



Fig. 2. **Qualitative results of our dynamic 3D reconstructions which are used for tracking.** For each object, the right visualization shows every 3D point in a given tracklet in world-space. The left visualization shows the 3D reconstruction obtained when mapping each of these points into object-centric space defined by our homogeneous motion transformations. Every point in our set of tracklet masks is present in both visualizations.

with rigid body transformations. This assumption is valid for cars, but not for pedestrians which can move in an articulated manner. Despite this, our 3D tracklet merging algorithm based on the calculation of these rigid-body transformations performs very well for pedestrians. As visualized in Figure 2, although our method cannot capture the fine-grained details of the articulated motion, it can still accurately capture the overall object motion which is what is required for tracking. Our long-term tracking is able to reduce the number of ID switches by around 50% compared to the initial 2D tracking results. Furthermore, our method has between 60% and 70% less ID switches than the previous best competing methods ([33] and [38]), using the same set of detections. This shows that our method successfully creates long-term tracks that are consistent even through occlusion, which is of utmost importance in many practical applications such as autonomous vehicles.

MOTSFusion extrapolates the 3D motion of object reconstructions both forward and backward in time to perform long-term tracking. Thus, this method works in an offline time-windowed setting. However, such a reconstruction-based tracking approach can be adapted to work online for use in applications such as autonomous robotics.

We make the following contributions. (i) We present a novel long-term tracking pipeline that uses dynamic 3D object reconstructions to merge tracks through long periods of occlusion. (ii) We present a method for recovering missed detections of objects based on their 3D motion obtained from 3D reconstruction. (iii) We present a thorough experimental evaluation validating the effectiveness of our reconstruction-based tracking showing that our approach achieves state-of-the-art performance for both bounding box and segmentation mask tracking on the KITTI dataset.

II. RELATED WORK

Tracking-by-Detection. Multi-Object Tracking (MOT) has been tackled by many approaches. Many successful methods have followed a tracking-by-detection paradigm [7], [46], [18], [8], [27], [23], [37], [15], [35], [1]. There exists many different approaches to the tracking-by-detection data-association problem, from network flow [46], to multi-hypothesis tracking [18], quadratic pseudo boolean optimization [8] and conditional random fields [7], [27]. We adopt the tracking-by-detection paradigm for MOTSFusion, taking

as input bounding box detections and attempting to merge them over time into consistent object tracks. To perform this merging, we propose a novel two-stage data-association algorithm which first creates short tracklets using 2D motion consistency, before merging these into long-term consistent object tracks using 3D motion consistency of dynamic object reconstructions.

Hierarchical Tracking. Previous work [15], [17], [9] has shown that tracking can be effectively performed in a tracklet-based multi-stage approach. Our method follows such a paradigm; first building up short tracklets using 2D image space motion consistency, followed by a second stage which merges these tracklets into long-term consistent tracks using 3D motion.

Segmentation-based Tracking. It is now possible to obtain segmentation masks for objects instead of just bounding boxes [13]. A number of recent papers [38], [28], [20] have exploited the use of pixel-precise masks for improving tracking, often using optical flow [16] or scene flow [41] to model the motion of each pixel. We adopt both of these techniques using both optical flow and scene flow within an object segmentation mask to determine motion consistency in both 2D and 3D.

Tracking in 3D. Tracking in 3D is invaluable for applications such as autonomous vehicles. Therefore, there has been a large body of research [27], [28], [33], [14], [21], [25] in this area. Most methods [27], [33] track using 3D bounding boxes and rely on simple motion cues such as average scene flow vectors. A few methods [14], [25] have tried to track object reconstructions in 3D by determining the precise transform for an object between frames. Our method follows a similar idea, however unlike previous methods that used techniques like ICP [5] for aligning point-cloud representations, our approach is able to directly optimize for an alignment of points whose correspondences are given by optical flow.

Dynamic Object Reconstruction. Dynamic object reconstruction is closely related to MOT, as to perform reconstruction first tracking needs to be performed. A number of methods [2], [31] have approached this task. Our MOTSFusion algorithm also performs this task and calculates accurate dynamic object reconstructions, as visualized in Figure 2, however our differentiating factor is that our method finishes

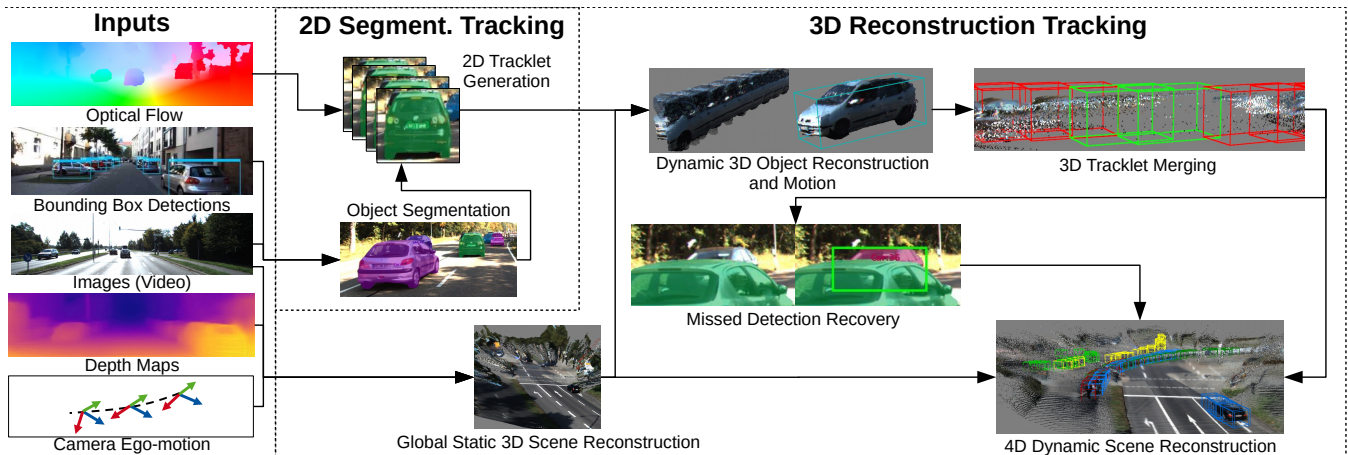


Fig. 3. **Overview of the proposed MOTSFusion method.** Given a set of inputs typical for autonomous driving applications, our method performs tracking in a two stage pipeline. First tracklets are formed using 2D image space motion consistency from optical flow and segmentation masks. Secondly 3D world-space motion consistency is used to merge tracklets together into accurate long-term tracks while recovering missed detections. This is performed by calculating the precise 3D transforms that result in a dynamic 3D object reconstruction for each object.

the loop; using these reconstructions to in turn further improve the tracking result.

III. OUR APPROACH

MOTSFusion is built upon three key ideas. (i) Accurate short tracklets can be constructed using the 2D motion consistency obtained from segmentation masks and optical flow [20], [38]. This results in a large number of highly precise short tracklets for when objects are contiguously visible. (ii) For an object undergoing only rigid-body transformations, there exists a set of such transformations that fuses all of the point clouds of this object from each timestep into a consistent 3D reconstruction, and these transformations define the 3D motion of that object. (iii) Even for non-rigid objects, the approximate rigid-body transformations obtained by finding the best-fit 3D object reconstruction, results in 3D motion estimates which are accurate enough to determine the overall 3D motion of an object, and to determine if two tracklets have consistent 3D motion and should be merged into one longer track.

Following these three ideas, we present MOTSFusion (shown in Figure 3), a two stage algorithm which first creates short tracklets using the 2D motion consistency of segmentation masks under an optical flow warp, and then fuses these tracklets, using depth and ego-motion estimates, into consistent dynamic 3D object reconstructions. The transformations required for these reconstructions are then used to estimate the 3D motion of object tracklets, merging them into longer tracks if they undergo consistent 3D motion, and using the extrapolated positions to fill in detections where they were missed. MOTSFusion simultaneously tracks objects as both image space segmentation masks and world-space 3D object reconstructions. An example of 3D merging and interpolation is shown in Figure 4. A number of 3D object reconstruction results are shown in Figure 2.

Tracking Inputs. MOTSFusion uses video frames as input, as well as per frame ego-motion and depth estimates. We use stereo depth from DispNet3 [16], and ego-motion from

a SLAM algorithm ORB-SLAM2 [26]. MOTSFusion is designed to work with any available depth estimates (stereo, LiDAR, RADAR, SfM or single-image depth) and ego-motion estimates (SLAM, GPS, IMU). We use stereo and SLAM as these are commonly available for many applications and benchmarks. For object detection, we use both the recurrent rolling convolution (RRC) detector [29] and Track R-CNN [38]. We also use an optical flow estimate for each frame obtained from FlowNet3 [16].

Bounding Boxes to Segmentation Masks. The first step of MOTSFusion is to estimate a segmentation mask for each bounding box detection. We use a fully convolutional neural network from [20] which we call BB2SegNet. This crops and resizes an image region given by a bounding box to a 385×385 patch and outputs a segmentation mask for each detected box.

2D Tracklet Generation. Given object segmentation masks and forward optical flow for each pixel, we generate tracklets using a simple merging procedure. For each segmentation mask, we warp the pixels of this mask using the optical flow values at these pixels into the next frame. We calculate the IoU (intersection over union) for these warped masks and the set of segmentation masks in the next frame to create association similarities. We use the Hungarian algorithm to assign masks to previously existing tracklets. All masks that are not merged into previous tracklets begin new tracklets. A minimum IoU threshold is required to merge masks.

4D Scene Reconstruction. In order to obtain 3D object motion, we need the 3D location of each object in each timestep in a common world-frame. For our world-frame we use the position of the camera in the first frame and create a 4D (3D + time) point cloud of the scene using depth d_t , camera intrinsics $K \in R^{3 \times 3}$ and camera position matrix $T_t \in R^{4 \times 4}$ (the homogeneous transformation matrix of the accumulated ego-camera position over time) with the following equations:

$$(x, y, z)^C = ((u, v, 1) \times (K^{-1})^T) \cdot d_t \quad (1)$$

$$(x, y, z, 1)^W = (x, y, z, 1)^C \times T_t^\top \quad (2)$$

where (u, v) is the pixel location at time t , $(x, y, z)^C$ is the 3D point corresponding to pixel (u, v) in the current camera frame and the $(x, y, z)^W$ is the 3D point in the world frame. We can now estimate object motion independent of camera motion. The scene reconstruction is used for visualization of the 3D tracking (Figure 1).

Dynamic 3D Object Fusion. We calculate a set of rigid-body transforms that warp the set of 3D points for an object tracklet in each time-step into a consistent 3D object reconstruction. We fit a homogeneous transform from the world-space points within a pixel-mask from time t to the world-space points within the pixel-mask of the same tracklet at time $t + 1$. This transformation is accumulated over all timesteps so that all points in an object tracklet are warped into a consistent 3D reconstruction.

In order to minimize the influence of incorrect depth estimates and object masks, we filter the set of 3D points used to fit the transform by calculating the local outlier factor LOF_k [6] using the local reachability density lrd_k of each point p with its k nearest neighbors N_k . The local reachability density uses the reachability distance rd_k , which is defined by the Minkowski distance d_{min} between two points \mathbf{p} and \mathbf{q} and the k -distance d_k of q , which is the maximum of the Minkowski distances of the k nearest neighbors of q , as follows:

$$rd_k(\mathbf{p}, \mathbf{q}) = \max\{d_k(\mathbf{q}), d_{min}(\mathbf{p}, \mathbf{q})\} \quad (3)$$

$$lrd_k(\mathbf{p}) := 1 / \left(\frac{\sum_{\mathbf{q} \in N_k} rd_k(\mathbf{p}, \mathbf{q})}{|N_k(\mathbf{p})|} \right) \quad (4)$$

Using the local reachability distance of each point, we can compute the local outlier factor LOF_k [6] by:

$$LOF_k(\mathbf{p}) := \frac{\sum_{\mathbf{q} \in N_k} \frac{lrd_k(\mathbf{q})}{lrd_k(\mathbf{p})}}{|N_k(\mathbf{p})|} \quad (5)$$

Subsequently, we filter out points with a higher LOF_k than the median LOF_k of all points. For the remaining 3D points at time t and $t + 1$, we use the optical flow vector to correlate points between the two timesteps. We further filter these points to only those for which correspondences exist between the two timesteps. We then sample a maximum of 200 corresponding points uniformly over the mask area.

On these points we perform a non-linear least-squares optimization to determine the homogeneous transform that best aligns the two 3D point clouds. We restrict this transform to be a 3-DoF homogeneous transform (X and Z translation, and rotation around the ground plane normal). The assumptions of this limited transform are valid for KITTI as the ground-plane is approximately flat. We parametrize the 3D rigid motion with $\xi \in \mathfrak{se}(2)$, the Lie algebra associated with $SE(2)$, which is a minimal representation for this motion. We use a non-linear least-squares optimizer to fit this transform by minimizing the $L2$ distance between each pair of corresponding points in the two point clouds. This transform gives the precise alignment (motion) of an object between timesteps in world coordinates. For each tracklet, we calculate this transform for all pairs of neighboring

frames and accumulate the transforms, merging the point clouds from every timestep into one 3D reconstruction in a consistent object-centric reference frame. Results of this are shown in Figure 2, where it is evident that our transforms are highly accurate, even when accumulated over many timesteps.

3D Tracklet Merging. Tracklets are merged by analyzing their 3D consistency under the motion given by the object fusion. Objects can then be tracked through long periods of complete occlusion, significantly reducing ID switches. We extrapolate the motion prediction of each tracklet 20 frames beyond the tracklet’s temporal extent, and measure the motion consistency between tracklets while taking into account the inherent uncertainty in these extrapolations. Although object alignment is often accurate and fits well, this is not always the case, e.g. under heavy partial occlusion. We estimate the 3D alignment accuracy, to determine whether a motion estimate is suitable for estimating overall object motion.

To measure the alignment accuracy, we use the residual error of the fitted homogeneous transform. To calculate the expected object motion after the end of a given tracklet, it is important to only use highly accurate motion (alignment) estimates. The estimates should represent the object’s motion at the end of the tracklet and should contain information from as many timesteps as possible. We define the ‘Trusted Motion Region’ (TMR) as the set of contiguous motion transforms (requiring at least two that are contiguous) closest to the end of the tracklet which are all below a residual error threshold. From this TMR, we calculate an expected object motion. We map each of the transforms from a global coordinate frame into an object-centric coordinate frame that moves as the object moves. We average the motions in this coordinate system to estimate the objects’ overall motion, and extrapolate this relative to the new object location in each timestep. Note that it is not possible to meaningfully average or extrapolate homogeneous transforms in global coordinates, they must first be transformed into a coordinate system that moves with the object.

For this, we have to estimate an object’s absolute location relative to which this mapping can be applied. Although we have estimated accurate local transformations from one timestep to the next, the absolute position of the object is still uncertain. To model this we use an uncertainty estimate that comes from stereo estimation. For a given timestep, we model the object center point with its given uncertainty using a multivariate normal distribution, with the expected object center point \mathbf{p} as the median location of our filtered 3D point set for the object mask in that time step, and the uncertainty represented as the covariance, Σ , obtained using forward error propagation [12]:

$$\Sigma = (\mathbf{F}_L(\mathbf{p}) \Sigma_{\text{pix}}^{-1} \mathbf{F}_L(\mathbf{p}) + \mathbf{F}_R(\mathbf{p}) \Sigma_{\text{pix}}^{-1} \mathbf{F}_R(\mathbf{p}))^{-1}, \quad (6)$$

where $\mathbf{F}_L(\mathbf{p}), \mathbf{F}_R(\mathbf{p}) \in \mathbb{R}^{4 \times 4}$ are Jacobians (evaluated at \mathbf{p}) of the left and right camera projection matrices, respectively. The matrix $\Sigma_{\text{pix}} = (\sigma_u \ 0; 0 \ \sigma_v)$ models uncertainty in the pixel measurements, with σ_u and σ_v both set to 0.5. Now

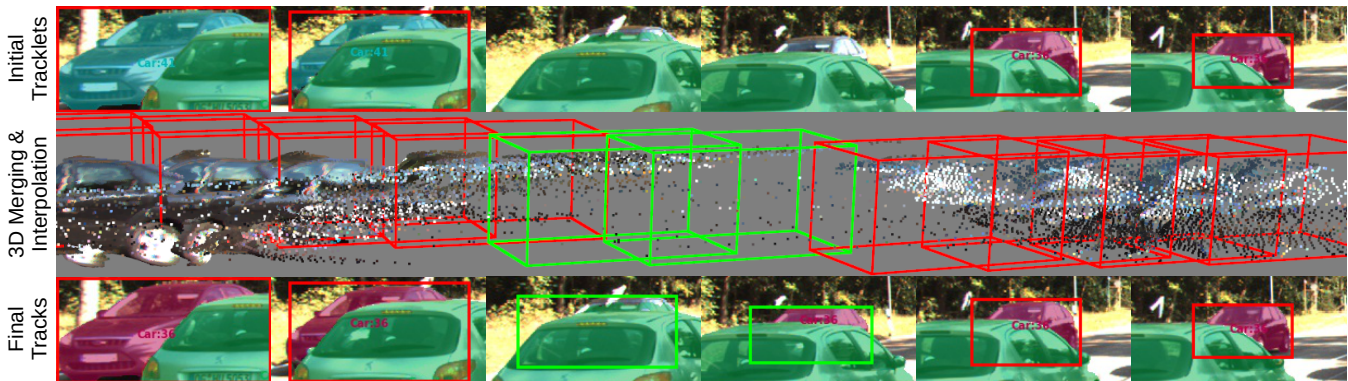


Fig. 4. **Example of our 3D tracklet merging and missing detection filling** Top: Initial 2D bounding box detections (red) and segmentation based tracklet results. Middle: Result of our interpolated 3D bounding boxes between the two tracklets, showing the temporal consistency of the two tracklets 3D motion through the frames with no detections. Bottom: Original 2D bounding box detections (red) and the new interpolated 2D bounding boxes (green) together with the filled segmentation mask and merged track ID.

that we have an estimate for the object center \mathbf{p} , we map the motion transform ξ from global coordinates into object-centric coordinates $\hat{\xi}$, centered at the current \mathbf{p} , using the following formula:

$$\begin{pmatrix} \hat{\xi}_x \\ \hat{\xi}_y \\ \hat{\xi}_z \\ \hat{\xi}_\theta \end{pmatrix} = \begin{pmatrix} \cos(\xi_\theta) - 1 & -\sin(\xi_\theta) & \xi_x \\ \sin(\xi_\theta) & \cos(\xi_\theta) - 1 & \xi_z \\ 0 & 0 & \xi_\theta \end{pmatrix} \begin{pmatrix} \mathbf{P}_x \\ \mathbf{P}_z \\ 1 \end{pmatrix} \quad (7)$$

This object-centric motion parametrization ($\hat{\xi}$) encodes the same motion transformation as the original (ξ) transform, but now is centered on the moving object center. This allows us to meaningfully average these object relative transformations, as well as to extrapolate them into the future, always relative to the current object center estimate. The object-centric expected motion is then calculated as the average object-centric motion ($\hat{\xi}$) from within the Trusted Motion Region. The estimated extrapolated object position at each timestep is calculated by taking \mathbf{p} from the timestep closest to the end of the tracklet, and extrapolating the motion using $\hat{\xi}$ in each timestep. The uncertainty of this estimate is also updated each timestep using Equation 6. We use the extrapolated object motion and uncertainty to estimate the 3D motion consistency between two tracklets and to measure the likelihood that these tracklets belong to the same object. For a pair of potentially merging tracklets (where one tracklet begins within 20 frames of the other ending), we extrapolate both tracklets' 3D motion towards each other into all timesteps between the Trusted Motion Regions of the two tracklets, including the last frame of the earlier TMR and the first frame of the later TMR. From these 3D position estimates and their uncertainties, the 3D motion consistency of two tracklets is given by the average Mahalanobis distance of these 3D position estimates weighted by their respective uncertainties from the covariances Σ (Eq. 6). If the extrapolated motion beyond the end of one of the tracklets cannot be estimated robustly (because two contiguous motion transforms with residuals lower than a threshold are not present), we determine the 3D motion consistency of the two tracklets by only extrapolating one towards the other and only computing the consistency in the timestep of the last

frame of the tracklet for which we have no motion estimate. If both tracklets do not have a robust motion estimate, then both are assumed to be stationary. If the 3D motion consistency between two tracklets is higher than a threshold, these tracklets are merged into one track.

Missing Detection Recovery. For frames between merged tracklets, we then attempt to determine if the object being tracked is actually present in this frame (and was simply a missed detection that should be filled), or was actually occluded and should not be assigned a 2D bounding box or segmentation mask.

To do this, we first estimate a rough 3D bounding box for each 3D object center \mathbf{p} . We use \mathbf{p} as the bounding box center and assume a fixed width/height/length for pedestrians and cars given by the average width/height/length of the 3D bounding boxes in the KITTI 3D detection training set. Using a fixed sized bounding box greatly simplifies the 3D detection problem (compared to [42]) and results in adequate localization for producing segmentation mask proposals. We set the bounding box orientation θ to the direction of motion if the object undergoes significant motion. Otherwise, we set θ to the direction of the eigenvector with the largest eigenvalue for all of the bird's eye view 3D points for the object's current timestep (this gives the direction of the greatest variance of the 3D points). Examples of these 3D bounding boxes can be seen in Figure 1.

Once we have the 3D bounding box estimated from the motion extrapolation, we then project this 3D bounding box back into image space as a 2D bounding box and combine it with the previous-frame bounding box corners warped by the median optical flow vector of all points in the bounding box. Next, we run our BB2SegNet to get a segmentation mask for this bounding box. We then run a check on the validity of this new segmentation mask by taking the points within the new mask and projecting them back into 3D world coordinates using their per pixel depth estimate and Equation 1 and 2. If the 3D points of the new mask are sufficiently close to the 3D bounding box center, then the mask passes the consistency check. This check determines if the object has been occluded, since in this case the points belonging to

Tracking	Detect.	Segm.	Speed	Cars					Pedestrians				
				sMOTSA	MOTSA	IDS	FP	FN	sMOTSA	MOTSA	IDS	FP	FN
Ours	RRC[29]	BB2SegNet[20]	0.44	85.7	94.5	31	44	364	-	-	-	-	-
Ours (no fill)	RRC[29]	BB2SegNet[20]	0.43	85.6	94.3	31	37	386	-	-	-	-	-
Ours (2D)	RRC[29]	BB2SegNet[20]	0.14	85.2	94.0	61	37	386	-	-	-	-	-
BePix[33]	RRC[29]	BB2SegNet[20]	0.36	84.9	93.8	97	61	337	-	-	-	-	-
Oracle	RRC[29]	BB2SegNet[20]	-	86.9	95.9	0	3	330	-	-	-	-	-
Ours	TrRCNN[38]	BB2SegNet[20]	0.44	82.8	90.5	51	51	661	59.4	72.6	35	99	784
Ours (no fill)	TrRCNN[38]	BB2SegNet[20]	0.43	82.6	90.2	51	41	695	58.8	71.8	35	94	814
Ours (2D)	TrRCNN[38]	BB2SegNet[20]	0.14	81.9	89.6	102	41	695	58.2	71.2	55	94	814
Oracle	TrRCNN[38]	BB2SegNet[20]	-	87.0	96.0	0	19	303	68.7	86.0	0	29	440
Ours	TrRCNN[38]	TrRCNN[38]	0.44	78.2	90.0	36	94	673	50.1	68.0	34	181	855
Ours (no fill)	TrRCNN[38]	TrRCNN[38]	0.43	78.1	89.8	36	86	699	49.5	67.2	34	178	886
Ours (2D)	TrRCNN[38]	TrRCNN[38]	0.14	77.5	89.2	85	86	699	48.9	66.6	53	178	886
BePix[33]	RRC[29]	TrRCNN[38]	0.36	76.9	89.7	88	280	458	-	-	-	-	-
TrRCNN[38]	TrRCNN[38]	TrRCNN[38]	0.50	76.2	87.8	93	134	753	46.8	65.1	78	267	822
CAIWT[27]	TrRCNN[38]	TrRCNN[38]	0.28	68.1	79.4	106	333	1214	42.9	61.0	42	401	863
CAMOT[28]	TrRCNN[38]	TrRCNN[38]	0.76	67.4	78.6	220	172	1327	39.5	57.6	131	198	1090
Oracle	TrRCNN[38]	TrRCNN[38]	-	82.0	95.1	0	30	361	58.3	80.3	0	23	635

TABLE I

MASK TRACKING RESULTS ON KITTI MOTS VALIDATION. WE DO NOT EVALUATE THE RRC DETECTOR ON PEDESTRIANS, BECAUSE DETECTIONS ARE ONLY AVAILABLE FOR CARS. BEST RESULT NUMBERS PER SECTION IN **BOLD**. SPEED IS MEASURED IN SECONDS PER FRAME.

the new mask will be significantly in front of the estimated 3D bounding box. If the consistency check is passed, then it is very likely that the object given by this 3D bounding box, 2D bounding box and segmentation mask actually belong to the object being tracked, and as such are added to the tracking results. This effectively fills in missed detections while only introducing very few false positives. After running this infilling procedure between all merged tracklets, we also run it at the beginning and end of whole tracks, extrapolating beyond the track extent. We apply this procedure to every frame until we reach a frame where our consistency check fails, the object moves out of the camera field of view, or we reach the end of the video sequence.

IV. EXPERIMENTS

Datasets. In order to evaluate our reconstruction based tracking method we use the KITTI dataset [10]. This dataset contains scenes captured from a moving vehicle. We use the KITTI tracking benchmark to evaluate our bounding box tracking results on both cars and pedestrians in real-world driving scenes. Recently, the annotations for this dataset were extended with pixel-level mask annotations to evaluate the MOTS task (multi-object tracking and segmentation) [38]. We use both the official KITTI test server as well as the validation split from [38] to evaluate our tracking results. At the time of submission, only bounding boxes (without masks) were able to be evaluated using the test server, so MOTS results are only presented on the validation set.

Evaluation Metrics. We adopt the commonly used CLEAR-MOT [4] metrics to evaluate bounding box based multi-object tracking, the standard evaluation metrics for KITTI MOT [10]. For segmentation based tracking we adopt the segmentation adapted version of those from [38]. For bounding boxes the most important metric is MOTA, which incorporates three type of errors: false positives (FP), false negatives (FN) and ID switches (IDS)[4]. However, the definition of ID switches is not consistent between different tracking benchmarks. For MOTS (segmentations) we use the version

of IDS from [38] (also used in the MOTChallenge [24]). For MOT (bounding boxes) we present the original version from KITTI [10] as **MOTA**, however it has often been pointed out that this definition does not correctly account for ID switches [3], [34], [45], [22]. Hence, we also present results on the validation set using the definition from [38] and [24], which we label **MOTA***.

Specifically, **MOTA*** counts ID switches not only when a ground truth object has a different ID in frame t than in frame $t-1$, but also if a ground truth object has a different ID *over the whole sequence*. This interpretation of ID switches is denoted as **IDS*** in Table II. Since this is the standard metric for ID switches in the MOTS task, it is referred to simply as **IDS** in Table I for the MOTS evaluation.

For the MOTS (segmentation) task we use **MOTSA**, the segmentation version of MOTA. We also show results on **sMOTSA**, which takes the pixel accuracy of a mask into account by incorporating the IoU of a mask with the ground truth mask in the score.

Segmentation Tracking: Setup comparison. In Table I we present the evaluation results of MOTSFusion for segmentation mask tracking on the KITTI MOTS validation set. We compare results with three different combinations of detectors and segmentation methods. We use both the detections and segmentations from [38] for a fair comparison to the previous state-of-the-art for segmentation tracking. We also use a stronger detector [29] and a stronger segmentation method [20], so that we can compare the previous state-of-the-art bounding box tracking algorithm [33] with added segmentation masks. Finally, we report a combination of the detections from [38] with segmentations from [20]. We evaluate for both cars and pedestrians using detections from [38], and only for cars using detections from [29] (as pedestrian detections are not available). Using better detections and better segmentations does benefit our method. Using [20] segmentations instead of [38], sMOTSA increases from 78.2 to 82.8 for cars and from 50.1 to 59.4 for pedestrians (4.6 and 9.3 percentage point increase, respectively). Using [29]

Tracking	Speed	Cars					
		MOTA	MOTA*	IDS	IDS*	FP	FN
Ours (no fill)	0.43	94.0	93.7	9	31	45	400
Ours (2D)	0.14	93.9	93.3	12	58	45	400
BePix[33]	0.30	93.7	92.9	31	91	88	354
Oracle	-	95.8	95.8	6	6	0	371

TABLE II

BOUNDING BOX TRACKING RESULTS ON KITTI TRACKING VALIDATION (CARS). THE MOTA* AND IDS* METRICS USE THE ADAPTED IDS DEFINITIONS FROM [38]. ALL METHODS USE RRC DETECTIONS [29]. SPEED IS MEASURED IN SECONDS PER FRAME.

detections instead of [38], sMOTSA increases another 2.9 percentage points from 82.8 to 85.7 for cars.

Segmentation Tracking: Method ablation. In all five experimental setups, we present ablation results, showing how our 3D reconstruction-based tracking improves over the initial tracklets (*Ours (2D)*). With reconstruction-based tracklet merging only (*Ours (no fill)*), we reduce the IDS from 61 to 31 for cars and from 55 to 35 for pedestrians (49% and 36% relative improvement, respectively), while not changing the number of FPs and FNs. We observe similar results over all setups resulting in a sMOTSA increase of between 0.4 and 0.7 percentage points. This is a significant improvement in the method’s ability to perform long-term tracking. When also performing missed detection recovery (*Ours*), we reduce the number of FNs from 386 to 364 for cars and from 814 to 784 for pedestrians, while increasing the FPs only marginally from 37 to 44 for cars and from 94 to 99 for pedestrians. Again, we observe similar results over all setups resulting in a further sMOTSA increase of between 0.1 and 0.6 percentage points.

Segmentation Tracking: Comparison to state-of-the-art. Our tracker outperforms TrackR-CNN [38] with the same detections and segmentations by 2 percentage points for cars (78.2 vs. 76.2) and 3.3 for pedestrians (46.8 vs. 50.1) in sMOTSA, and has 61% (36 vs. 93) and 56% (34 vs. 78) less IDS for cars and pedestrians, respectively. When comparing to BeyondPixels [33] with added segmentations from BB2SegNet, we improve from 84.9 to 85.7 in sMOTSA while reducing the number of IDS from 97 to 31. This is less than a third of the IDS. Using the segmentation method from [38] our method also outperforms [33] by 1.3 percentage points in sMOTSA (78.2 vs. 76.9), even though [33] uses the stronger RRC detector. Our method also significantly outperforms other tracking methods [27] and [28] using the same detections and segmentations.

Segmentation Tracking: Oracle comparison. We also present results for each setup using an ‘oracle’ tracker, that takes the given detections and segmentations, and associates these into tracks using the ground-truth associations. Our best performing method for cars obtains a sMOTSA score of 85.7, which is only 1.2 percentage points below the theoretical maximum of a perfect tracking method. Note that the Oracle tracker still has FPs because the MOTSA evaluation script constrains all object masks within one frame to not overlap, thus even when only selecting masks that assign to ground truth masks, these can become unmatched when all of the

Tracking	Detect.	Speed	Cars			
			MOTA	IDS	FP	FN
Ours	RRC[29]	0.44	84.83	275	681	4260
BePix[33]	RRC[29]	0.30	84.24	468	705	4247
IMMDP[43]	FRCNN[30]	0.19	83.04	172	391	5269
PMBM[32]	Own	0.01	80.39	121	1007	5616
extraCK[11]	FRCNN[30]	0.03	79.99	343	642	5896
MCCPD[19]	FRCNN[30]	0.01	78.90	228	316	6713
JCSTD[36]	Regio[40]	0.07	80.57	61	405	6217
NOMT[7]	Regio[40]	0.09	78.15	31	1061	6421
LPSVM[39]	Regio[40]	0.02	77.63	130	1239	6393
SCEA[44]	Regio[40]	0.06	75.58	104	1306	6989
CIWT[27]	Regio[40]	0.28	75.39	165	954	7345

TABLE III

BOUNDING BOX TRACKING RESULTS ON KITTI TRACKING TEST (CARS). OUR METHOD ACHIEVES THE HIGHEST MOTA SCORE OF THE TEN BEST PERFORMING PUBLISHED METHODS ON THE KITTI TRACKING BENCHMARK. NOTE, THAT THE METHODS WITH FRCNN DETECTOR TRAIN THE DETECTOR DIFFERENTLY. SPEED IS MEASURED IN SECONDS PER FRAME.

masks computed from the bounding boxes of one frame are forced to be non-overlapping.

Bounding Box Tracking: Comparison to state-of-the-art. We also evaluate bounding box based tracking on the KITTI MOT test set and a validation split defined in [38]. The results for the validation split are shown in Table II and the results for the test set are shown in Table III. MOTSFusion outperforms the tracking result of BeyondPixels [33], the current best performing published method, on both sets by a significant margin, while using the same detections. It also outperforms other state-of-the-art methods that use different detections. According to the standard definition for IDS on KITTI MOT, we reduce the IDS compared to [33] from 31 to 9 on the validation split and from 468 to 275 on the test set. When evaluating with the more correct IDS* on the validation split, we are able to show that our method achieves a high long-term track consistency producing only 31 IDS*, whereas BeyondPixels produces a significantly higher number of 91 IDS*. We outperform BeyondPixels on the MOTA metric by 0.3% and 0.6% on the val/test split respectively, while outperforming it by 1.6% on the MOTA* metric on the val set. For bounding box tracking evaluation we do not perform the missing bounding box filling, as the checks that determine if a detection should be filled require checking against a segmentation mask of visible pixels, whereas the bounding boxes in KITTI MOT are ‘amodal’, which means that they cover both the visible and hidden parts of objects and cannot be validated with our mask-based checks.

Runtime. We measure the runtime of MOTSFusion per frame, for both preprocessing and each tracking stage of our algorithm. Calculating the per pixel optical flow and depth each take 0.07 seconds per frame. Calculating the relative camera pose between two frames takes 0.06 seconds. Thus the preprocessing time is 0.20 seconds per frame. Our 2D motion consistency based tracklet generation takes 0.07 seconds per frame to generate segmentation masks for all objects and to merge them into tracklets. The 3D motion

consistency based long-term tracklet merging and missed detection handling takes a total of 0.17 seconds per frame, of which 0.16 seconds are used to fit the homogeneous transforms for the 3D object fusion. The overall time for our algorithm is 0.44 seconds per frame. In comparison to other tracking algorithms, TrackR-CNN [38] takes 0.50 seconds per frame, and BeyondPixels [33] takes 0.30 seconds per frame (plus 0.06 seconds for mask generation for MOTs). Thus our algorithm is able to run with a similar efficiency while performing much better, especially for long-term tracking. Note that our method would get faster when using LiDAR or GPS as input because depth and/or ego-motion would come directly from a sensor. Note that, as is standard for MOT, the detector run-time is not included for any of the methods.

V. CONCLUSION

We have presented a framework in which both tracking and 3D object reconstruction can be performed together and can benefit from each other, with tracking enabling reconstruction, and reconstruction enabling long-term tracking through occlusions. In evaluations, our method outperforms previous tracking methods for both bounding box and segmentation tracking. In particular, our approach is able to track objects 'long-term' through complete occlusion or missed detections. We demonstrate a clear benefit of using 3D reconstruction to improve tracking, and present a tracking framework, MOTSFusion, where this can be exploited effectively and efficiently.

Acknowledgments. This project was funded, in parts, by ERC Consolidator Grant DeeVise (ERC-2017-COG-773161).

REFERENCES

- [1] M. Andriluka, S. Roth, and B. Schiele. People-tracking-by-detection and people-detection-by-tracking. In *CVPR*, 2008.
- [2] I. A. Bãrsan, P. Liu, M. Pollefeys, and A. Geiger. Robust dense mapping for large-scale dynamic environments. In *ICRA*, 2018.
- [3] J. Bento and J. J. Zhu. A metric for sets of trajectories that is practical and mathematically consistent. *arXiv:1601.03094*, 2016.
- [4] K. Bernardin and R. Stiefelwagen. Evaluating multiple object tracking performance: The clear mot metrics. *JIVP*, 2008.
- [5] P. J. Besl and N. D. McKay. On detection, data association and segmentation for multi-target tracking. *PAMI*, 1992.
- [6] M. M. Breunig, H.-P. Kriegel, R. T. Ng, and J. Sander. Lof: Identifying density-based local outliers. In *ACM SIGMOD*, 2000.
- [7] W. Choi. Near-online multi-target tracking with aggregated local flow descriptor. In *ICCV*, 2015.
- [8] A. Ess, B. Leibe, K. Schindler, and L. van Gool. A mobile vision system for robust multi-person tracking. In *CVPR*, 2008.
- [9] A. Geiger, M. Lauer, C. Wojek, C. Stiller, and R. Urtasun. 3d traffic scene understanding from movable platforms. *TPAMI*, 2014.
- [10] A. Geiger, P. Lenz, and R. Urtasun. Are we ready for autonomous driving? the kitti vision benchmark suite. In *CVPR*, 2012.
- [11] G. Gunduz and T. Acarman. A lightweight online multiple object vehicle tracking method. In *IVS*, 2018.
- [12] R. Hartley and A. Zisserman. *Multiple view geometry in computer vision*. Cambridge university press, 2003.
- [13] K. He, G. Gkioxari, P. Dollár, and R. Girshick. Mask r-cnn. In *ICCV*, 2017.
- [14] D. Held, J. Levinson, and S. Thrun. Precision tracking with sparse 3d and dense color 2d data. In *ICRA*, 2013.
- [15] C. Huang, B. Wu, and R. Nevatia. Robust object tracking by hierarchical association of detection responses. In *ECCV*, 2008.
- [16] E. Ilg, T. Saikia, M. Keuper, and T. Brox. Occlusions, motion and depth boundaries with a generic network for disparity, optical flow or scene flow estimation. In *ECCV*, 2018.
- [17] R. Kaucic, A. Perera, G. Brooksby, J. Kaufhold, and A. Hoogs. A unified framework for tracking through occlusions and across sensor gaps. In *CVPR*, 2005.
- [18] C. Kim, F. Li, A. Ciptadi, and J. M. Rehg. Multiple hypothesis tracking revisited. In *ICCV*, 2015.
- [19] B. Lee, E. Erdenee, S. Jin, and P.-K. Rhee. Multi-class multi-object tracking using changing point detection. In *ECCV Workshops*, 2016.
- [20] J. Luiten, P. Voigtlaender, and B. Leibe. Premvos: Proposal-generation, refinement and merging for video object segmentation. In *ACCV*, 2018.
- [21] W. Luo, B. Yang, and R. Urtasun. Fast and furious: Real time end-to-end 3d detection, tracking and motion forecasting with a single convolutional net. In *CVPR*, 2018.
- [22] A. Maksai, X. Wang, F. Fleuret, and P. Fua. Non-markovian globally consistent multi-object tracking. In *ICCV*, 2017.
- [23] A. Milan, S. Roth, and K. Schindler. Continuous energy minimization for multitarget tracking. *PAMI*, 2013.
- [24] L. Milan, A. Leal-Taix, K. Schindler, S. Roth, and I. Reid. Mot challenge, 2014.
- [25] D. Mitzel and B. Leibe. Taking mobile multi-object tracking to the next level: People, unknown objects, and carried items. In *ECCV*, 2012.
- [26] R. Mur-Artal and J. D. Tardós. Orb-slam2: An open-source slam system for monocular, stereo, and rgb-d cameras. *TRO*, 2017.
- [27] A. Ošep, W. Mehner, M. Mathias, and B. Leibe. Combined image- and world-space tracking in traffic scenes. In *ICRA*, 2017.
- [28] A. Ošep, W. Mehner, P. Voigtlaender, and B. Leibe. Track, then decide: Category-agnostic vision-based multi-object tracking. *ICRA*, 2018.
- [29] J. Ren, X. Chen, J. Liu, W. Sun, J. Pang, Q. Yan, Y. Tai, and L. Xu. Accurate single stage detector using recurrent rolling convolution. In *CVPR*, 2017.
- [30] S. Ren, K. He, R. Girshick, and J. Sun. Faster r-cnn: Towards real-time object detection with region proposal networks. In *NIPS*, 2015.
- [31] M. Runz, M. Buffier, and L. Agapito. Maskfusion: Real-time recognition, tracking and reconstruction of multiple moving objects. In *ISMAR*, 2018.
- [32] S. Scheidegger, J. Benjaminsson, E. Rosenberg, A. Krishnan, and K. Granström. Mono-camera 3d multi-object tracking using deep learning detections and PMBM filtering. In *IVS*, 2018.
- [33] S. Sharma, J. Ansari, J. Murthy, and K. Krishna. Beyond pixels: Leveraging geometry and shape cues for online multi-object tracking. In *ICRA*, 2018.
- [34] H. B. Shitrit, J. Berclaz, F. Fleuret, and P. Fua. Tracking multiple people under global appearance constraints. In *ICCV*, 2011.
- [35] S. Tang, M. Andriluka, B. Andres, and B. Schiele. Multiple people tracking by lifted multicut and person re-identification. In *CVPR*, 2017.
- [36] W. Tian, M. Lauer, and L. Chen. Online multi-object tracking using joint domain information in traffic scenarios. *TITS*, 2019.
- [37] Y. Tian, A. Dehghan, and M. Shah. On detection, data association and segmentation for multi-target tracking. *PAMI*, 2018.
- [38] P. Voigtlaender, M. Krause, A. Ošep, J. Luiten, B. Sekar, A. Geiger, and B. Leibe. Mots: Multi-object tracking and segmentation. *CVPR*, 2019.
- [39] S. Wang and C. Fowlkes. Learning optimal parameters for multi-target tracking with contextual interactions. *IJCV*, 2016.
- [40] X. Wang, M. Yang, S. Zhu, and Y. Lin. Regionlets for generic object detection. In *ICCV*, 2013.
- [41] A. Wedel, T. Brox, T. Vaudrey, C. Rabe, U. Franke, and D. Cremers. Stereoscopic scene flow computation for 3d motion understanding. *IJCV*, 2011.
- [42] X. Weng and K. Kitani. Monocular 3d object detection with pseudo-lidar point cloud. *arXiv:1903.09847*, 2019.
- [43] Y. Xiang, A. Alahi, and S. Savarese. Learning to track: Online multiobject tracking by decision making. In *ICCV*, 2015.
- [44] J. Yoon, C. Lee, M. Yang, and K. Yoon. Online multi-object tracking via structural constraint event aggregation. In *CVPR*, 2016.
- [45] S.-I. Yu, D. Meng, W. Zuo, and A. Hauptmann. The solution path algorithm for identity-aware multi-object tracking. In *CVPR*, 2016.
- [46] L. Zhang, L. Yuan, and R. Nevatia. Global data association for multi-object tracking using network flows. In *CVPR*, 2008.